Shape Control of Compliant, Articulated Meshes: Towards Modular Active-Cell Robots (MACROs)

Ahsan I. Nawroj, *Student Member, IEEE*, and Aaron M. Dollar, *Senior Member, IEEE*

***Abstract*—In this letter, we explore the shape control of compliant, articulated meshes created from shape memory alloy (SMA)-based linear actuators (Active Cells). These compliant meshes form the mechanical subsystem of a class of proposed modular active-cell robots (MACROs). Our "Active Cells" are centimeter-scale SMA actuators capable of ∼25% linear strain. The deformation of MACRO meshes in response to current inputs at the passive nodes are modeled and validated for accuracy in prior work. In this letter, we investigate an efficient and scalable control policy that allows us a given MACRO to be electrically-driven to achieve a specified shape. Validation experiments on a range of MACRO simulations establish a high degree of accuracy and repeatability of the controller. The control strategy is shown to be efficient and robust to variations in start- and target-shapes, and in mesh complexity.**

***Index Terms*—Cellular and modular robots, networked robots, simulation and animation.**

I. Introduction

DISCRETE material robots are an exciting field of research aimed towards creating redundant, high DOF articulable structures, such as deconstructible architecture in harsh climates, dynamically adjustable cranes for space applications, controllable-deformation airfoils, and others [1], [2]. Homogeneity of the constituent 'cells' allow the mechanisms to be robust to intermittent damage, customizable to fit changing task demands, and versatile in the range of tasks any given collection of cells can perform.

Towards this general goal, we have proposed a class of systems called Modular Active Cell robots (MACROs), which use compliant, articulated meshes of custom linear actuators called Active Cells [Fig. 1(a), (b)], as well as some external control circuitry, to create shape-changing robotic systems. In prior work, we described the design of Active Cells, as well as a scalable and predictive model of MACRO meshes constructed using these cells and passive compliant nodes [3]. Unlike classic approaches to the design of modular robots [4], MACRO modules are high degree-of-freedom (DOF) reconfigurable structures, and thus combinations of MACRO meshes to create larger MACROs allows incremental increase in the capabilities of the overall mechanism.

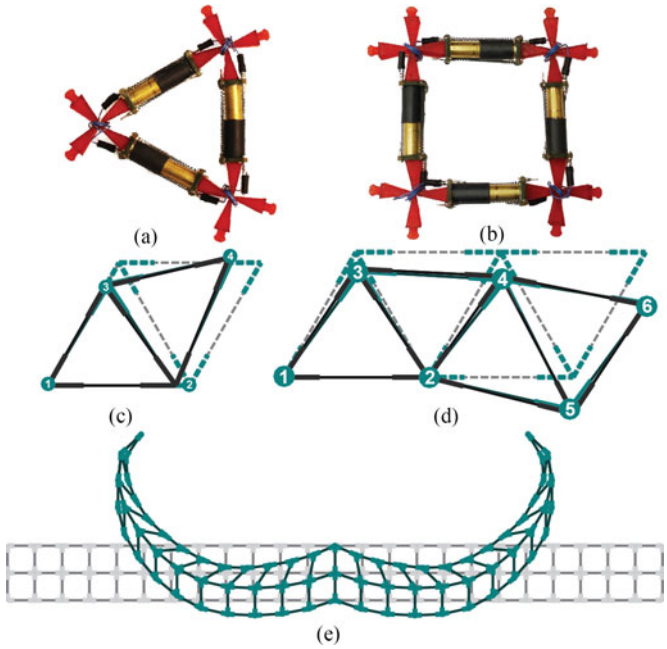

Fig. 1. (a), (b) Fabricated simple triangular and square MACRO meshes. (c), (d) Larger instances of MACRO models controlled to an arbitrary shape (starting configurations shown in dashed lines). (e) A large MACRO module demonstrating shape-control.

This approach to develop robotic structures is grounded in examples from biology. An analogous example to MACROs is the hierarchy of organs and tissues found in living organisms. An organ (such as the human heart) is a functional device that serves a specific set of tasks. The tissue from which the heart is made, however, is an abstract collection of subunits – cells. The type of cells present in the tissue, the connectivity and configuration of the cells and their method of activation dictates the performance of the tissue [5]. A tissue of cells can be used to create the lining of the stomach or the human heart by modifying the properties of the cells, their configuration, and control. MACROs operate under a similar premise: for a given task requiring a deformation, a set of MACROs must be used in a specified cell-connectivity and set of voltage inputs at the mesh nodes.

In this letter, we develop a two-tiered control strategy to address the task of actuating a MACRO mesh to match a given target shape (Fig. 1(c)–(e)). The algorithm is both computationally inexpensive and scalable, and can have wide-ranging impact

Manuscript received February 15, 2017; accepted May 28, 2017. Date of publication June 9, 2017; date of current version June 21, 2017. This letter was recommended for publication by Associate Editor N. Y. Chong and Editor A. Bicchi upon evaluation of the reviewers' comments. This work was supported in part by the National Science Foundation under Grant IIS-1317976 and in part by the Air Force Office of Scientific Research under Grant FA9550-11-1-0093. *(Corresponding Author: Ahsan I. Nawroj.)*

The authors are with the Department of Mechanical Engineering and Materials Science, Yale University, New Haven, CT 06520 USA (e-mail: ahsan.nawroj@yale.edu; aaron.dollar@yale.edu).

Digital Object Identifier 10.1109/LRA.2017.2714146

in centralized control of mobile robots, tensegrity structures, or lattice networks.

The rest of the letter is organized as follows: first, we situate our research in the field of shape-control of physical networks in Section II. We next describe both the physical system as well as a physically realistic computational model of the system in Section III to provide context for the control strategy. We provide a description of the two-tier algorithm in Section IV. We test the control strategy on simulated meshes and intuitive shape-change requirements in Section V, and repeat these tests in hardware (Section VI). We conclude with some discussion of the results of our validation experiments.

II. Related Work

Networked systems are common in both nature and engineered systems. The links in these networks may be physical or virtual, and all networked systems have some equivalent to link stiffnesses and equilibrium lengths. Several fields of research utilize network formulations to both design and control robotic mechanisms. A ready example of a similar problem is found in the formation control of mobile robots [6]. As the scale of this problem grows, decentralized solutions [7] tend to obtain faster convergence to desired configurations. Keeping communication networks invariant to the motion of network nodes is another challenge for mobile robots, addressed through maintaining network rigidity [8] or dynamically choosing between feasible configurations [9].

Similar control problems arise for tensegrity structures, where path control of network elements can be solved for simple configurations [10], and solved using genetically evolved controllers for cyclic paths in spatial mechanisms [11]. Among structures with position – or torque – controlled actuators, variable geometry trusses are good examples of related research [12]. Such truss manipulators have been shown to use torque control on low-order approximations [13], strain-control (e.g. for piezoelectric actuators) or indirectly controlled through the material in which the truss is embedded [14]. Finally, recent work on discrete materials closely resemble our own prior work, such as micro-architectured materials controlled by bulk stiffness relations [15], and shell-structures controlled by electro-active polymers [16].

In summary, there exists a wide variety of control strategies that have proven useful for networked systems, ranging from kinematic approaches for well-characterized systems to computationally-derived controllers with little knowledge of the model. The scalability and accuracy of control strategies also vary widely. Mobile-robot networks may involve tens of nodes and require high resolution control, whereas discrete materials use hundreds or thousands of nodes and require approximate control for bulk properties.

Our own contribution is aimed towards structures of both the small, discrete networks, as well as potentially much larger networks involving tens or hundreds of nodes. The proposed strategy assumes the use of a stiffness controlled actuator along edges of the mesh with a known mapping from voltage/current inputs to stiffness change. We experimentally obtain the mapping for our actuators (Active Cells), but this can be replicated for any stiffness actuator.

This approach can be compared to strut/cable control of tensegrity structures [11], where selections of mesh elements are actuated. Since MACRO meshes can potentially activated all edges to some degree for shape control, selective approaches do not easily translate to our system. An approach similar to ours is found in [17], where stiffness is controlled in a mechanical structure directly; this approach uses selective connection between elements of the mesh as the control variable, which is distinguished from our approach of routing power through the network. We believe for large structures of compliant elements our approach achieves similar performance without sacrificing bulk strength.

The minimal assumptions we make about actuators in the control formulation lead an algorithm that may be generalized to several of the cited research fields, specifically tensegrity structures and homogeneous modular robots.

III. Mesh Components and Models

The mechanical component of MACROs is a mesh of custom linear actuators (Active Cells) connected by passive compliant nodes. In the following sections, the term MACRO is used to refer to this mechanical mesh, ignoring the electronics that drives voltages at the node terminals. This allows us to isolate the control algorithm from the implementation of the electronics specific to our MACRO instance. MACRO components are simplified in the model used for the control algorithm, separating the algorithm from the physical prototypes. This provides opportunity in the future to generalize the specific form of the hardware components without modifying the controller. Note that the control algorithm developed using the simplified models are expected to be applicable to our hardware prototypes with minimal modifications. This is considering prior work that establishes that the simplified model accurately predicts the behavior of hardware MACRO meshes [3].

The Active Cells we use in MACRO construction (Fig. 2(a)) are contractile elements made from two Nitinol shape-memory alloy (SMA) extension coils in parallel with a biasing steel compression spring. A cell is activated by current flow through the SMA coils, where joule heating causes a material transition from martensitic to austenitic SMA. There exists a controllable change in the shear modulus of the material from temperature variations, which causes a change in the elastic stiffness of the coils. As the stiffness of the Nitinol coils is varied, the elastic equilibrium of the parallel Nitinol-steel-spring system shifts to minimize the mechanical energy of the cell. The Active Cell thus acts as a variable stiffness actuator in response to applied current. The design of our Active Cell is described in detail in [18]. Design variations in Active Cells can be instituted through changes in SMA wire diameter, overall coil diameter, shape-setting methods for Nitinol, and bias-spring properties. Relevant design parameters following prior design optimization [19] are listed on Table I.

Nodes in a MACRO mesh are formed using passive compliant flexures (Fig. 2(b)). Electrical connectivity to all cells connected

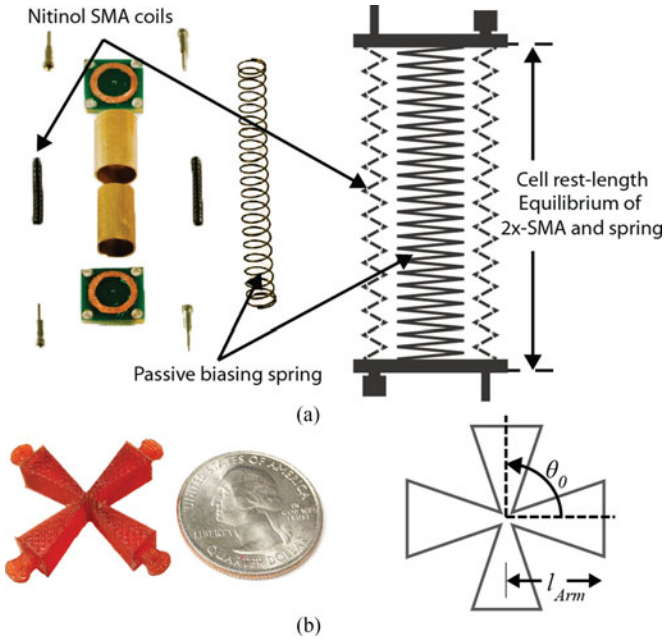

Fig. 2. Components of any MACRO module: (a) Active Cells and (b) passive nodes (prototypes on left, models on right).

TABLE I
PROPERTIES OF ACTIVE CELLS

Property	Symbol	Value
Cell equilibrium length		25.1 mm
Bias-spring rest length	$l_{0-\text{Spring}}$	35 mm
Bias spring stiffness	k_{Spring}	0.142 N/mm
Nitinol coil rest length	$l_{0-\text{Nitinol}}$	9.14 mm
Nitinol min stiffness	$k_{\text{Martensite}}$	0.0302 N/mm
Nitinol max stiffness	$k_{\text{Austenite}}$	0.7189 N/mm
Cell electrical resistance	R_N	1.5 Ω

to the node is accomplished with thin hookup wire external to the node (Fig. 1(a), (b)). Since the cells are electrically resistive Nitinol elements, the set of node voltage inputs fully specifies the electrical power flow in a MACRO.

Formally, let us consider a MACRO mesh containing *M* Active Cells and *N* passive nodes, organized as a graph *G* of edges as node tuples *(i, j)* with an adjacency matrix $A \in \mathbb{R}^{N\times N}$, where $A_{ij} = 1$ iff a cell is connected between nodes *i* and *j*. We define an edgewise adjacency matrix $A_e \in \mathbb{R}^{M\times N}$:

$$A_{eij} = \begin{cases} 1 & \exists\ (i,j) \in G,\ i < j \\ -1 & \exists\ (i,j) \in G,\ i > j \\ 0 & \text{else} \end{cases} \tag{1}$$

The node positions of an Active Cell can then be described as the elastic equilibrium of the nitinol coils and the bias springs for a given stiffness of the nitinol coils:

$$x_{eq}\left(k_N\right) = \underset{x}{\operatorname{argmin}} \begin{pmatrix} \frac{1}{2}\ k_N\left(A_e x - l_{0N} - l_{\text{node}}\right)^2 \\ +\frac{1}{2} k_s\left(A_e x - l_{0s} - l_{\text{node}}\right)^2 \end{pmatrix} \tag{2}$$

where x_{eq} is the cartesian position vector between the two nodes connected to the cell, k_N the stiffness of the Cell's nitinol coils (summed total for the parallel coils), $\Delta x = A_e x$ the distance from x_i to x_{i+1}, l_{0N} the rest-length of the Nitinol coils, k_s the stiffness of the biasing spring, l_{0s} the rest-length of the biasing spring, and l_{node} the length of the arms of a node. Since a MACRO is simply a collection of Active Cells and passive nodes connecting them, the shape of a MACRO is fully defined if all such x_{eq} are known. The complete shape of the MACRO (set of all x_{eq}, written X_{eq}) is:

$$X_{eq}\left(K_N\right) = \underset{X}{\operatorname{argmin}} \begin{Bmatrix} \frac{1}{2} K_N \left(A_e X - L_{0N}\right)^2 \\ +\frac{1}{2} K_s \left(A_e X - L_{0s}\right)^2 \\ +\frac{1}{2} \kappa_\theta \left(\theta - \theta_0\right)^2 \end{Bmatrix} \tag{3}$$

In the equation above, the variables K_N, K_S and κ_θ are the set of k_N, k_S and κ_θ for all cells. The three terms in the equation of equilibrium node positions correspond to, respectively, the mechanical deformation energy contributed by the Nitinol coils, the passive springs, and the torsional stiffness of compliant nodes.

The complexity of MACROs grows with the size and complexity of the mechanisms they aim to emulate. To design and control complex networked mechanisms, we used experimental data on individual Active Cells and nodes to create an accurate and scalable model of the system. This physically realistic simulation has been validated against vision-based shape-matching of simple fabricated MACROs [3]. In validating the proposed shape-controller, we use this model of the MACRO system, thus abstracting the underlying hardware system with a generalizable model.

IV. PATH SEGMENTATION AND SHAPE CONTROL

From a shape-control perspective, MACROs with many cells are difficult structures to control since arbitrary compliant networks can have many degrees-of-freedom that cannot be directly controlled from voltage inputs at the network nodes. Exceptions to this statement are triangulations and other 'rigid' isostatic networks, the subject of considerable existing research [8], [20]. We chose to consider more general networks than triangulations since non-rigid networks have much larger deformation workspaces, increasing the capability of any given MACRO. In this letter, we study mesh configurations that correspond to 2 of the 3 regular tilings of the plane: the square and the triangle. This allows us to compare the controller's performance on both a 'rigid' and a 'floppy' configuration. The choice of mesh configuration repeating units ("mesh primitives") is a non-trivial one, and is explored in concurrent research.

In the following sub-sections, we describe the modeling assumptions used in shape control, configuration variables appropriate to the problem, and the shape control algorithm.

A. Model Assumptions and Terminology

Although the entire set of node positions is necessary to completely describe the shape of the MACRO, the shape of the MACRO that interacts with the environment is described by the

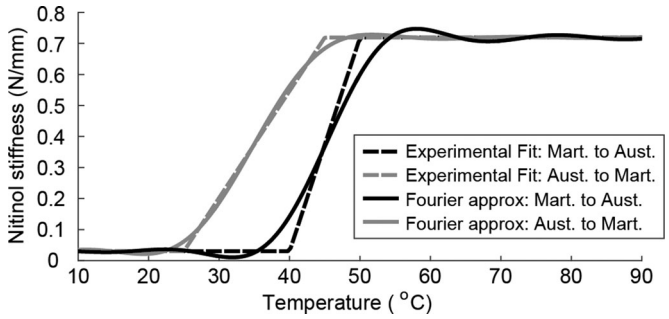

Fig. 3. Experimental mapping from temperature to stiffness for Nitinol coils. Two continuous 6th order Fourier series are fit to each of the hysteresis curves for use in the analysis of Active Cell response to control inputs.

positions of only the nodes at the boundary of the MACRO. Specifically, the node positions can be written as:

$$X_{eq} = \{X_I \cup X_B\}_{eq} \tag{4}$$

In any given control task, the interior nodes X_I may not be fully specified initially since they do not contribute to the description of the essential shape. If the user does specify these positions, they can be incorporated into the computation of the controller. The boundary node positions X_B define the shape of the MACRO, and they must be known for both starting and target configurations to compute control signals. We assume that in test conditions, the user inputs the complete node position set. We further assume that all position vectors are on a frictionless plane.

The controllable variable in (3) are the cell stiffnesses, written K_N. We use these stiffnesses as the configuration variable for our control scheme. The cell stiffnesses are a sufficient descriptor of the required shape change, since the start and target shapes can be written as:

$$K_0 = \underset{k}{\operatorname{argmin}} \{X_0 - X_{eq}(k)\} \tag{5}$$

$$K_f = \underset{k}{\operatorname{argmin}} \{X_f - X_{eq}(k)\} \tag{6}$$

Each of these stiffnesses are functions of the temperatures of the coils, written $K_N = f(T)$. The mapping *f(T)* is non-linear, with a noticeable hysteresis, and is experimentally determined for a given coil geometry and memory-shape setting. A piecewise linear fit to the experimentally determined map as well as a continuous Fourier approximation of the mapping is shown in Fig. 3. This mapping can be varied by varying the geometry and fabrication procedure of the Nitinol coils, and a study establishing these variations can be found in [21]. We assume that this mapping is identical for all cells.

We can write the SMA stiffness change as a function of the applied electrical power across the cells with some approximation in low-loss thermal conduction:

$$\frac{d}{dt}(K_N) = \frac{d}{dt}(f(T))\frac{dT}{dt} = \frac{P f'(T)}{m_N c_N} \tag{7}$$

Here the constants m_N and c_N are the mass of the Nitinol coils and the specific heat capacity of Nitinol respectively. Since the mapping *f(T)* can be approximated locally for each hysteresis curve by a Fourier series, an approximate derivative of the mapping can be obtained and (5) can be computed for any given temperature and stiffness. The electrical power *P* dissipated across the cells (each of resistance R_N), connected in the graph *G*, is:

$$P = \frac{(\Delta V)^2}{R_N} = \frac{(A_e V)^2}{R_N} \tag{8}$$

For a quasi-static system, we write the cell stiffness change as a function of the applied power over time interval Δt:

$$P = \frac{m_N c_N}{f'(T)\Delta t}(K_N - K_{N0}) \tag{9}$$

This relationship between a desired stiffness change and requisite cell power dissipation is obtained by relatively few assumptions and relates cell stiffnesses to node voltages.

B. Path Segmentation and Discretization

The proposed control algorithm involves two steps: a preprocessor that plans and segments the path through the configuration (stiffness) space and a configuration controller that sets voltage levels at the nodes of the network to control the stiffness. The overall algorithm is shown in Fig. 4.

Note that since for a given target shape, specified as a set of node positions of dimension $(N \times 2)$, and control inputs at the nodes of the network of dimension $(M \times 1)$, where in general $M < 2N$, the system is under-actuated. The preprocessor maps the starting and target shapes to a space of *M* dimensional stiffnesses. For small changes in stiffness, the corresponding change in positions is assumed to be small.

The purpose of the preprocessor is to describe a path through the configuration (stiffness) space that traverses the locally smooth manifold of the configuration space. While most target configurations will lie outside an immediate neighborhood of the starting configuration, the local smoothness of the configuration manifold can be used to construct an appropriate segmentation preprocessor to the control algorithm. An *r*-step segmentation of the path (K_0 to K_f) is defined to be an interpolation that generates *r* intermediate configurations to the desired target, $S = K_0, K_1 \ldots, Kf$, where $|S| = r$. The simplest segmentation is the uniform-step linear interpolation, written:

$$S = \{K_i : i = 0, \ldots, r\}, \quad K_i = K_0 + i/r\,(K_t - K_0) \tag{10}$$

For small MACROs, linear segmentation is sufficient to achieve the target configuration in a few steps. In our testing of small MACROs, we used linear segmentation with *r* ranging from 2 to 5. The pre-processor essentially splits the control problem into *r* separate and simpler control problems, which are solved sequentially, to provide control inputs that drive the configuration of the MACRO to the *r* intermediate K_i. For each segment *i*, the starting and target stiffnesses K_{i-1} and K_i are computed by the preprocessor, and the configuration controller is called to obtain the correct node voltage inputs to affect this stiffness change.

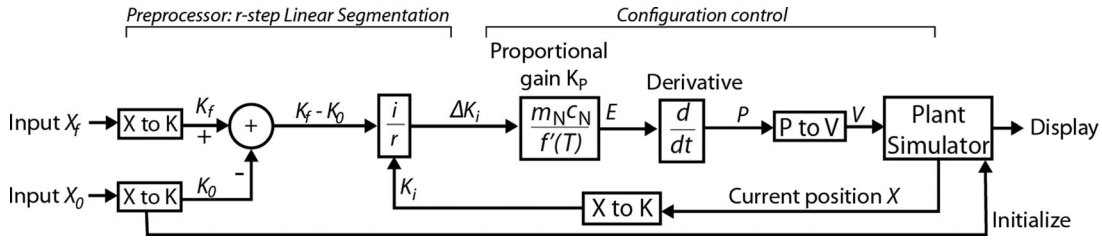

Fig. 4. Block diagram for the overall control policy.

C. Shape Matching and Configuration Control

If the starting and target shapes of the MACRO can be fully specified by the stiffness of the Active Cells, (9) can map the desired shape change directly to power inputs. The following equations describes this heuristic strategy of obtaining the necessary power dissipation (P^*) for a given pair of starting (K_0) and target (K_f) configurations of the MACRO:

$$P^* = \frac{m_N c_N}{f'(T)\,\Delta t}\,(K_f - K_0) \tag{11}$$

Equation (8) can be reversed for a network to obtain the corresponding voltage inputs (V^*) by using the minimization:

$$V^* = \underset{V}{\operatorname{argmin}} \left\{ P^* - \frac{(A_e V)^2}{R_N} \right\} \tag{12}$$

In summary, for a chosen time-interval, any shape change can be mapped to a corresponding change in cell stiffnesses, which can be used to compute power dissipation across the cells and the corresponding voltage inputs required. The equations above are phrased as minimizations of necessarily convex functions, and thus are rapidly solvable.

The shape change (X_0 to X_f) is described using the space of node positions ($N \times 3$ in space) while the corresponding stiffness space has a dimension ($M \times 1$), where it is possible that $M < N$. Thus, the mapping from shape change to stiffness change is not unique, and could potentially pass through stiffness-space singularities. The phenomenon can be ameliorated by appropriately segmenting the desired stiffness change (K_0 to K_f) into smaller steps that can be uniquely mapped to shape variations. Stiffness-space singularities are only hypothesized by the matrix form of the system, and are not explored in this letter. In future work, we will explore the possibilities of creating singular configurations as well as segmentation paths to avoid these configurations.

A final consideration for the proposed control strategy is discretization. The voltage input to the nodes is essentially driven by a PD controller with a specific proportional gain ((11)), and thus the selection of the discrete time-steps at which the algorithm is updated, Δt, affects the convergence properties significantly. To choose this time step appropriately, we look at the notoriously low bandwidth of Nitinol coils. From our experimental trials, we have found that Δt of up to 2 s is sufficient to converge the controller reliably. In validating the controller, we chose a Δt of 1 s to provide more robust convergence. A sample of this entire controller simulation is shown on Figs. 5 and 6. A plot of the controller evaluation metric for this trial is shown on Fig. 7.

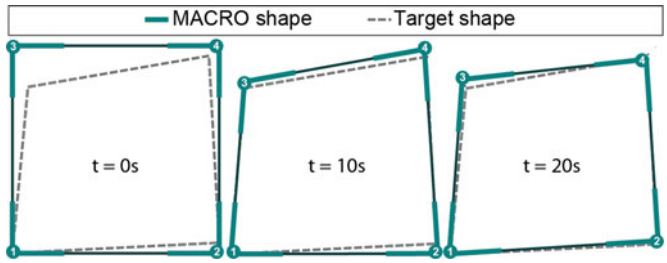

Fig. 5. Test of control strategy on a small MACRO square mesh. The shape of the mesh (solid lines) is shown to converge to the target shape (dotted lines). All edges of this mesh are Active Cells.

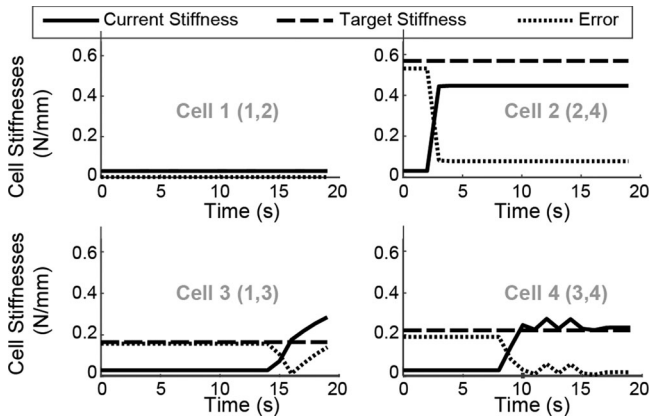

Fig. 6. Plot of each configuration variable (stiffness) for trial of small MACRO square mesh. The desired stiffness is plotted over the trial time as well (dashed lines). The errors at each time is plotted in dotted lines. Note that for all cells, the configuration error decreases over time. The configuration error for cell 3, however, shows the controller diverting away from the desired target configuration to decrease area-IOU error.

V. Validation of Control in Simulation

We tested our control algorithm on simulated MACROs of varying scale and complexity. To illustrate the variables tracked in our analysis, consider a small MACRO mesh. The results of applying our control strategy on this square MACRO with four Active Cells is shown in three frames in Fig. 5. The error metric used by the controller is the 2-norm of stiffnesses between a MACRO configuration and the desired configuration (Fig. 6). Since the eventual goal of the controller is to deform the MACRO mesh to match the shape of the target mesh, we also

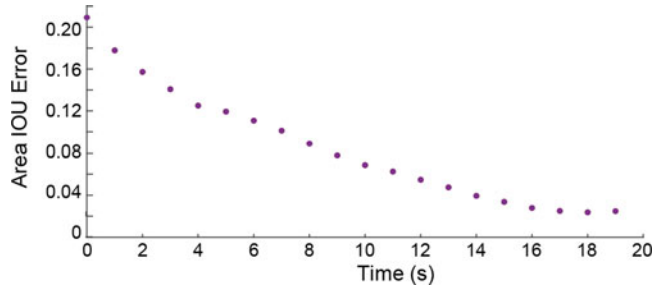

Fig. 7. Plot of shape-match errors (IOU error) for trial of small MACRO square mesh.

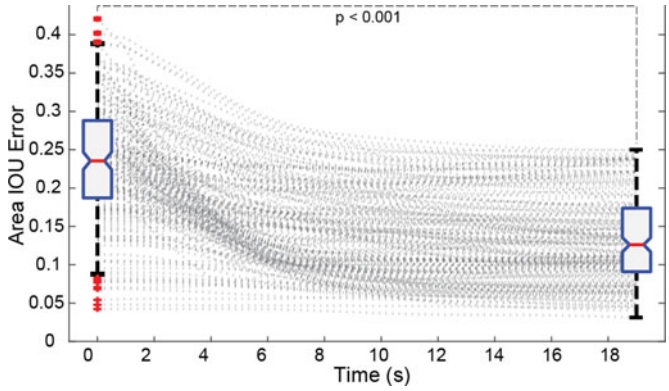

Fig. 8. Error (IOU) for all simulation trials over time shown in gray dotted lines. Distribution of errors at start and end of trials is shown in box-plots. Note decrease in errors despite high variance in starting errors.

define a mesh shape-matching error: The Intersection-Over-Union (IOU). The Intersection-Over-Union error (E_{IOU}) for this problem is defined for a given mesh positions *X(t)* and the desired shape X_f by:

$$E_{IOU} = 1 - \frac{(X(t) \cap X_f)_{\text{Area}}}{(X(t) \cup X_f)_{\text{Area}}} \tag{13}$$

The shape-match error for this example trial of a small MACRO is shown in Fig. 7. As the trial progresses, the shape-match error metric decreases, and this corresponds to the iteration steps of Fig. 5.

The test conditions for validation included 100 MACROs using triangles as the mesh primitive and 100 MACROs using squares. For each mesh connectivity in these trials, the target position for the controller was set by deforming the nominal mesh by a random scaling factor between [0.75, 1] and a random bend angle between [0, 10] degrees. Gaussian noise with signal-to-noise ratio of between [20, 30] dB was added after these transformations to the target shape.

The result of these simulated trials in aggregate is shown in Fig. 8. Note that the starting IOU error (at time $t = 0$) is normally distributed about a mean of 0.23 ± 0.08. The final IOU error for all trials are closer to *0*, at a distribution with mean of 0.13 ± 0.06. The decrease in IOU error is statistically significant with $p < 0.001$.

In our analysis, we first study whether the performance of the controller is different for different lattice types. It can be

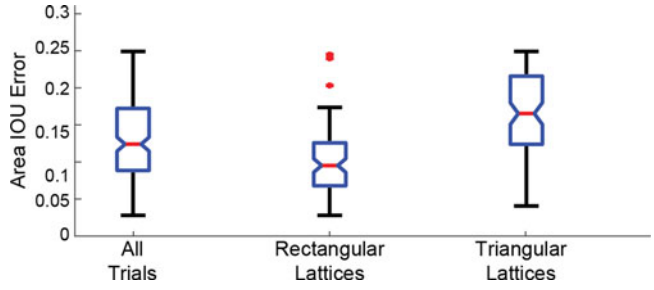

Fig. 9. The final IOU error for all trials compared to data segments for each lattice type. Note no statistical difference exists between the performance of the controller for lattice types.

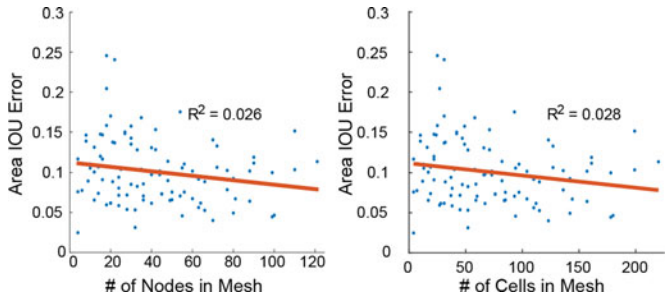

Fig. 10. The final IOU error for all trials plotted against (a) the number of cells and (b) the number of nodes in the mesh. No correlation is found between the steady-state error for the controller as the complexity of the network grows.

seen on Fig. 9 that no statistical difference exists ($p < 0.01$) between the steady-state error of the controller for the two lattice types studied. While this does not preclude potential lattice dependence of the controller, it does suggest that the controller can deform MACROs from a nominal starting shape to at least *10%* of an arbitrarily set target shape.

The second analysis of the trial data is for mesh complexity. We plot the IOU error against the number of cells and the number of nodes in Fig. 10. No significant correlation was found for either case, suggesting the controller's steady-state errors are independent of the connective complexity of the MACRO mesh.

VI. Validation of Control in Hardware

Alongside the extensive study of the controller's performance in matching a target shape from a given shape, we conducted simple hardware trials of the controller. Since the MACRO mesh model was created using properties of the prototyped Active Cells and nodes, we hypothesize that a shape-controller controlling a simulated mesh would show comparable performance in the hardware equivalent of the same mesh. In prior work, we have validated the model in isolation using a simple square, Fig. 1(b).

To validate the controller's performance in hardware, we tested the controller on a start and target shape goal for a two-triangle mesh, shown in Fig. 11. The hardware equivalent of this mesh is shown in the background. The controller performance in 3 time steps is shown for the MACRO. Notice that the hardware system achieves comparable steady-state shape-match errors to the simulation, with the area IOU error

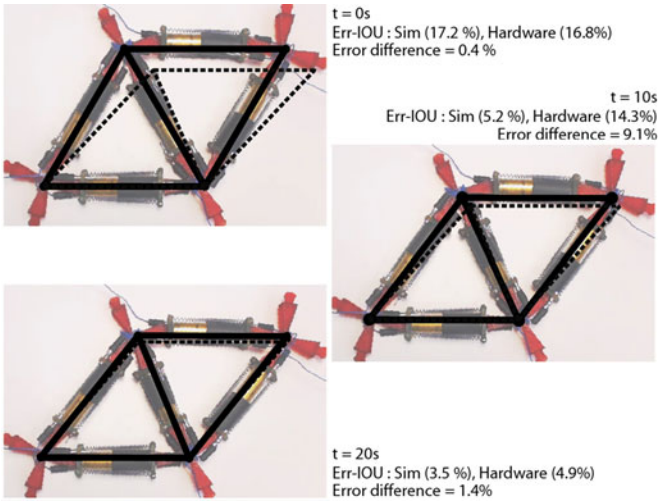

Fig. 11. A two-triangle MACRO mesh shape controlled to the specified target shape in simulation and in hardware (target shape shown in dashed lines; simulation output shown in solid lines). The shape-match error for the simulation and hardware trial (representative trial of five) is shown on the right.

for the simulated MACRO at 3.5%, and the area IOU error for the hardware MACRO at 4.9% ($\pm 1\%$, $n = 5$). Note that performance match between the hardware trial and the simulation is high at the end of the trial (within 1.9% of each other), but the match is low at the $t = 10$ s mark, suggesting effects of unmodeled transient behavior.

This preliminary hardware testing serves to demonstrate the realistic performance of the controller. Despite using a simplified model of the system, the controller is able to shape-control a given MACRO mesh from a starting shape to an arbitrary target shape within its workspace.

VII. Conclusion

We have developed a computationally inexpensive and robust policy to control the shape of a MACRO. We used the physics of our custom stiffness actuators (Active Cells) to design a preprocessor to the MACRO network such that MACRO shape can be controlled readily with a PD controller. We tested the controller on a large number of scale-varying MACRO modules to establish the accuracy and robustness of the control algorithm. We also validated the controller on a simple hardware MACRO mesh and established comparable performance to the simulation tests. In future work, we aim to study the effect of significantly varying the mesh primitives on the performance of the shape-controller, as well as the performance of the preprocessor in planning around stiffness-space singularities.

References

[1] K. C. Cheung and N. Gershenfeld, "Reversibly assembled cellular composite materials," *Science*, vol. 341, no. 6151, pp. 1219–1221, Sep. 2013.
[2] T. A. Schaedler *et al.*, "Ultralight metallic microlattices," *Science*, vol. 334, no. 6058, pp. 962–965, Nov. 2011.
[3] A. I. Nawroj, J. P. Swensen, and A. M. Dollar, "Toward modular active-cell robots (MACROs): SMA cell design and modeling of compliant, articulated meshes," *IEEE Trans. Robot.*, vol. 33, no. 4, 2017.
[4] M. Yim *et al.*, "Modular self-reconfigurable robot systems [grand challenges of robotics]," *IEEE Robot. Autom. Mag.*, vol. 14, no. 1, pp. 43–52, Mar. 2007.
[5] M. E. Silverman, D. Grove, and C. B. Upshaw, "Why does the heart beat? The discovery of the electrical system of the heart," *Circulation*, vol. 113, no. 23, pp. 2775–2781, Jun. 2006.
[6] K. Kanjanawanishkul, "Formation control of mobile robots: Survey," *Eng. Ubu. Ac. Th*, vol. 4, no. 1, pp. 50–64, 2011.
[7] A. Jadbabaie, J. Lin, and A. S. Morse, "Coordination of groups of mobile autonomous agents using nearest neighbor rules," *IEEE Trans. Autom. Control*, vol. 48, no. 6, pp. 988–1001, Jun. 2003.
[8] T. Eren, P. N. Belhumeur, B. D. O. Anderson, and A. S. Morse, "A framework for maintaining formations based on rigidity," *IFAC Proc. Vol.*, vol. 35, no. 1, pp. 499–504, 2002.
[9] J. P. Desai, V. Kumar, and J. P. Ostrowski, "Control of changes in formation for a team of mobile robots," in *Proc. Int. Conf. IEEE Robot. Autom.*, May 1999, vol. 2, pp. 1556–1561.
[10] Y. Moon, C. D. Crane, and R. G. Roberts, "Reverse kinetostatic analysis and stiffness synthesis of a spatial tensegrity-based compliant mechanism," *Mech. Mach. Theory*, vol. 70, pp. 320–337, Dec. 2013.
[11] C. Paul, F. J. Valero-Cuevas, and H. Lipson, "Design and control of tensegrity robots for locomotion," *IEEE Trans. Robot.*, vol. 22, no. 5, pp. 944–957, Oct. 2006.
[12] K. Miura, H. Furuya, and K. Suzuki, "Variable geometry truss and its application to deployable truss and space crane arm," *Acta Astronaut.*, vol. 12, no. 7/8, pp. 599–607, 1985.
[13] B. A. Boutin, A. K. Misra, and V. J. Modi, "Dynamics and control of variable-geometry truss structures," *Acta Astronaut.*, vol. 45, no. 12, pp. 717–728, Dec. 1999.
[14] B. K. Wada, J. L. Fanson, and E. F. Crawley, "Adaptive structures," *J. Intell. Mater. Syst. Struct.*, vol. 1, no. 2, pp. 157–174, Apr. 1990.
[15] L. A. Shaw and J. B. Hopkins, "An actively controlled shape-morphing compliant microarchitectured material," *J. Mech. Robot.*, vol. 8, Nov. 2015, Art. no. 21019.
[16] P. Lochmatter and G. Kovacs, "Design and characterization of an actively deformable shell structure composed of interlinked active hinge segments driven by soft dielectric EAPs," *Sens. Actuators A, Phys.*, vol. 141, no. 2, pp. 588–597, 2008.
[17] B. Haghpanah, H. Ebrahimi, D. Mousanezhad, J. Hopkins, and A. Vaziri, "Programmable elastic metamaterials," *Adv. Eng. Mater.*, vol. 18, no. 4, pp. 643–649, Apr. 2016.
[18] J. P. Swensen, A. I. Nawroj, P. E. I. Pounds, and A. M. Dollar, "Simple, scalable active cells for articulated robot structures," in *Proc. Int. Conf. IEEE Robot. Autom.*, 2014, pp. 1241–1246.
[19] A. I. Nawroj, J. P. Swensen, and A. M. Dollar, "Design of mesoscale active cells for networked, compliant robotic structures," in *Proc. Int. Conf. IEEE/RSJ Intell. Robot. Syst.*, 2015, pp. 3284–3289.
[20] T. Eren *et al.*, "Rigidity, computation, and randomization in network localization," in *Proc. IEEE INFOCOM*, 2004, vol. 4, pp. 2673–2684.
[21] J. P. Swensen and A. M. Dollar, "Optimization of parallel spring antagonists for Nitinol shape memory alloy actuators," in *IEEE Int. Conf. Robot. Autom.*, pp. 6345–6349, 2014.